

ORIGINAL ARTICLE

Open Access



# Integrated real-time precise point positioning system with B2b/B2a/B1C services

Zhetao Zhang<sup>1,2,3\*</sup> , Hao Wang<sup>1,2,3</sup> and Yuanxi Yang<sup>2,4</sup>

## Abstract

Real-Time Precise Point Positioning (RTPPP) technology is one of the most important means of positioning and navigation, whereas this type of service requires Internet access. As an alternative, satellite-based RTPPP can be utilized, especially for the PPP-B2b service of the BeiDou Navigation Satellite System (BDS). However, there is no systematic study on how to fully employ all satellite-based augmented services such as B2b, B2a, and B1C services in BDS. To ensure the continuity and availability of the PPP-B2b service, an Integrated Real-Time PPP (InRPPP) system is proposed which consists of B2b, B2a, B1C, and broadcast ephemeris messages. Specifically, the satellite orbit and clock errors are corrected by the B2b and B2a services, and the ionospheric delays by the B1C services. That is, the B2b, B2a, B1C, and broadcast ephemeris messages are resiliently utilized in the InRPPP system. Both static and kinematic experiments under complex conditions are carried out. The results indicate that compared to the PPP based on B2b, B2a, or B1C services, the InRPPP system performs the best in terms of visible satellite numbers and Position Dilution of Precision (PDOP) values. Also, in the static experiment, the InRPPP mode achieves the highest accuracy and the shortest convergence time compared to the PPP based on B2b, B2a, or B1C services. The Three-Dimensional (3D) Root-Mean-Square (RMS) value of the InRPPP mode is 0.49 m, improving 59.6% on average. For the convergence time, 65.9% improvements can be obtained on average. In the kinematic experiment, for the InRPPP solutions the jumps are suppressed and the availability and stability are increased, which exhibiting average 34.3% improvements in terms of the 3D RMS value. In conclusion, the InRPPP system with B2b/B2a/B1C services presents superior performance and has a great potential in real applications.

**Keywords** GNSS, Real-time PPP, PPP-B2b, BDSBAS-B2a, BDSBAS-B1C

## Introduction

Unlike traditional differential Global Navigation Satellite System (GNSS) technology, Precise Point Positioning (PPP) can achieve excellent accuracy using a standalone receiver (Jin & Su, 2020; Li et al., 2015; Malys & Jensen, 1990; Zumberge et al., 1997; Zhang et al., 2014; Zhang

et al., 2021). However, PPP accuracy is contingent upon the precision of clock and orbit products which restrict real-time availability (Zhang et al., 2023) and other problems such as ambiguity of carrier phase and multipath (Ge et al., 2008; Geng et al., 2013; Li et al., 2020; Zeng et al., 2023; Wang et al., 2024). To address the challenges of Real-Time PPP (RTPPP), an open-access Real-Time Service (RTS) has been launched since 2013, which is not accessible in the areas without Internet (Elsobeiey et al., 2016).

Different from the Internet-based RTPPP, the PPP-B2b service, known as the satellite-based RTPPP, is a feature service provided by BeiDou Navigation Satellite System (BDS). This service employs a regional monitoring network to calculate the corrections of satellite orbit, clock,

\*Correspondence:

Zhetao Zhang  
zt.zhang@hotmail.com; ztzhang@hhu.edu.cn

<sup>1</sup> State Key Laboratory of Geo-Information Engineering and Key Laboratory of Surveying and Mapping Science and Geospatial Information Technology of MNR, CASM, Beijing 100036, China

<sup>2</sup> State Key Laboratory of Spatial Datum, Xi'an 710054, China

<sup>3</sup> School of Earth Sciences and Engineering, Hohai University, Nanjing 211100, China

<sup>4</sup> Xi'an Research Institute of Surveying and Mapping, Xi'an 710054, China

and Differential Code Bias (DCB). These corrections are transmitted through Geostationary Equatorial Orbit (GEO) satellites to the users in the Chinese mainland and adjacent regions to provide centimeter-level real-time positioning accuracy (CSNO, 2020a; Yang et al., 2019, 2021b, 2022). Therefore, the PPP-B2b service overcomes the limitations imposed by network conditions and has been extensively utilized in Positioning, Navigation, and Timing (PNT) service (Ge et al., 2023; Tang et al., 2022; Xu et al., 2021), ocean positioning (Geng et al., 2022), seismic monitoring (Yang et al., 2021a; Zang et al., 2024), and meteorology (Yang et al., 2023). Similar to BDS, both Quasi-Zenith Satellite System (QZSS) and Galileo Satellite Navigation System (Galileo) also offer PPP services, namely the Centimeter Level Augmentation Service for QZSS (Kim et al., 2022), and the High Accuracy Service for Galileo (Kan et al., 2024; Naciri et al., 2023).

Recent studies have extensively evaluated and improved the PPP-B2b service, which mainly includes three aspects. First, the precision of B2b messages is systematically evaluated (Liu et al., 2022a, 2022b; Nie et al., 2021; Tao et al., 2021; Zhang et al., 2022). These studies demonstrate that the precision of B2b orbit and clock corrections is better than that with broadcast ephemeris but worse than the precise product and RTS corrections. The B2b DCB corrections are also more accurate than the broadcast Time Group Delay (TGD) corrections. Second, besides Dual-Frequency (DF), PPP-B2b has been extended to Single-Frequency (SF), triple-frequency, and five-frequency (Lan et al., 2022; Yang et al., 2024; Zhou et al., 2022). Third, some refinement schemes are proposed to improve the PPP-B2b service. Liu et al. (2022a, 2022b) and Sun et al. (2023) identified a constant bias in B2b clock corrections and found that both the accuracy and convergence time can be enhanced by correcting the bias. This satellite-specific clock bias can be estimated with a single station and transmitted via short-message communication to the users (Yuan et al., 2025). Also, Xu et al. (2023) improved the performance of the PPP-B2b service by estimating additional parameters in the mathematical model. Otherwise, B2b messages face some challenges, like message latency and mismatching, and incontinuity of corrections, which may decrease the availability of B2b messages (Liu et al., 2022a, 2022b; Ouyang et al., 2023). The BeiDou Satellite-Based Augmentation System (BDSBAS) has also been embedded into the BDS constellation, which can provide B1C and B2a services (Yang et al., 2022). The B1C service can augment GPS L1 C/A SF signal and provide satellite orbit, clock, and ionospheric corrections, while the B2a service augments GPS L1 and L5, and BDS B1C and B2a DF signals and provides satellite orbit and clock corrections (CSNO, 2020b, 2022; Chen et al., 2022). Limited studies, however, have

found that SBAS corrections can be applied to PPP mode (Heßelbarth et al., 2013; Li et al., 2016; Zhao et al., 2016), while the integration of BDSBAS and PPP modes needs further study (Yang et al., 2022; Zhang et al., 2025).

To ensure the continuity and availability of B2b messages and improve the PPP-B2b service, an Integrated RTPPP (InRPPP) system is proposed based on the ideal of resilient PNT (Yang, 2019). In the InRPPP system, B2b and B2a messages can be employed to correct satellite orbit and clock errors, and B1C and broadcast ephemeris messages to ionospheric delays. Thus, the InRPPP system can resiliently utilize the B2b, B2a, B1C, and broadcast ephemeris messages as well, which increases the number of redundant observations, making full use of the available augmentation messages, thus improving the positioning performance. Specifically, the method for correcting satellite orbit and clock errors, and atmospheric delays using B2b, B2a, and B1C services and the concept and procedure of the InRPPP system are first introduced in detail. Then, both static and kinematic experiments are conducted to assess the InRPPP system under complex conditions. Finally, the property of the InRPPP system is analyzed in terms of visible satellite numbers, Position Dilution of Precision (PDOP) values, accuracy, and convergence time.

## Methodology

In this section, we first outline the method for correcting satellite orbit errors, clock offsets, and atmospheric delays using B2b, B2a, and B1C services. Then, the concept of the InRPPP system with B2b, B2a, and B1C services is proposed, where the specific procedures are illustrated in detail. Last, the efficiency of the InRPPP mode is validated by assessing positioning accuracy in the PPP mode using various messages.

### Correction messages of B2b, B2a, and B1C services

BDS is designed to provide PPP-B2b service, which can broadcast satellite orbit, clock, and DCB corrections.

**Table 1** Information on B2b messages

Contents	Associated types	Issue of data	Nominal validity (s)
PRN mask	1	IOD SSR, IODP	–
Orbit correction	2, 6, 7	IOD SSR, IODN, IOD Corr	96
DCB correction	3	IOD SSR	86,400
Clock correction	4, 6, 7	IOD SSR, IODP, IOD Corr	12
URAI	2, 5, 6, 7	IOD SSR	96

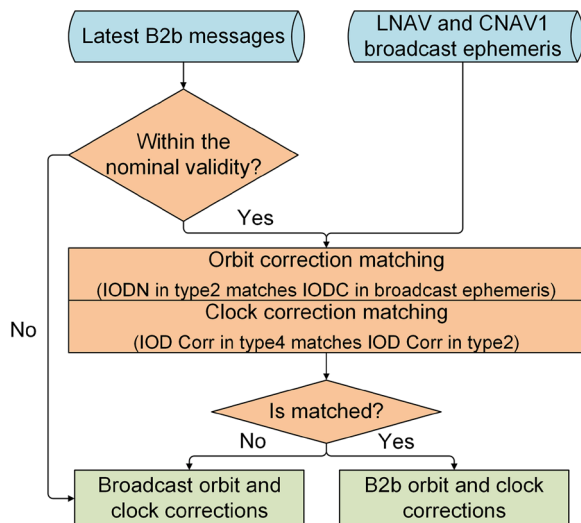
**Fig. 1** Matching strategy of B2b messages

Table 1 shows the information on B2b messages, along with the Issue of Data (IOD) and nominal validity and Fig. 1 shows a detailed matching strategy of B2b messages with those of the broadcast ephemeris. Specifically, B2b messages can only augment the GPS LNAV and BDS CNAV1 ephemeris messages. After correct matching, the B2b satellite orbit, clock, and DCB corrections can be calculated in Types 2, 4, and 3, respectively (CNSO, 2020a).

In addition, BDSBAS provides SF and Dual-Frequency Multi-Constellation services, known as B1C and B2a services, respectively. The B2a service augments GPS and BDS satellites and is intended for the DF users which can only be applied to GPS LNAV and BDS CNAV2 ephemeris messages. Note that CNAV1 and CNAV2 ephemeris messages differ in only two parameters: Signal-in-Space Monitoring Accuracy Index (SISMAI) and Inter-Signal Correction (ISC). Specifically, CNAV1 broadcasts ISC between C1D and C1P signals, while CNAV2 broadcasts ISC between C5D and C5P signals. Thus, CNAV1 can also be used in the B2a service theoretically. Table 2 shows main information on B2a messages. It is worth

noting that the variable means that the timeout interval is not fixed and depends on other messages. If B2a messages are within the timeout interval, we can obtain B2a satellite orbit and clock corrections by using Type 32 and CNAV1 broadcast ephemeris (CNSO, 2022; EUROCAE, 2019).

Different from the B2a service, the B1C service can only be used to augment the GPS L1C/A signal, broadcasting the corrections of orbit error, clock offset, and ionospheric delay. Table 3 shows the information on B1C messages. Fast corrections (Type 2–5) address the rapidly changing part of satellite clock offsets, and long-term corrections (Type 25) address satellite orbit, clock offset, and clock drift. Using Types 2 to 5 and Type 25, we can get B1C orbit and clock corrections. To mitigate the ionospheric delay, Type 26 provides the satellite-independent Vertical Delay (VD) values at ionospheric grid points which can be used to get B1C ionospheric corrections (CNSO, 2020b; RTCA, 2016).

#### InRPPP system with B2b, B2a, and B1C services

The IF combination is typically employed in traditional PPP technology and can achieve good accuracy. But in complex environments, issues such as the lose lock of satellites, signal interruption, and reduction in the satellite numbers often occur, resulting in insufficient DF observations and mixed SF and DF observations. If only DF observations are used, the visible satellite numbers may be insufficient, significantly affecting accuracy and convergence time. Therefore, we prefer to use a mixed SF and DF positioning mode, where SF and DF IF observations are utilized together. The raw observation equations of mixed SF and DF observations can be written as (Li et al., 2019; Nie et al., 2020; Zang et al., 2020)

$$dP_{r,i}^{(s)} = \mathbf{I}_r^{(s)} \mathbf{x} + t_r - t^{(s)} + \xi_{r,i} - \xi_i^{(s)} + \Gamma_r^{(s)} T_r^z + I_{r,i}^{(s)} + \varepsilon_{r,i}^{(s)} \quad (1)$$

$$\begin{aligned} d\phi_{r,i}^{(s)} = & \mathbf{I}_r^{(s)} \mathbf{x} + t_r - t^{(s)} + \zeta_{r,i} - \zeta_i^{(s)} \\ & + \Gamma_r^{(s)} T_r^z - I_{r,i}^{(s)} + N_{r,i}^{(s)} + \epsilon_{r,i}^{(s)} \end{aligned} \quad (2)$$

**Table 2** Main information on B2a messages

Contents	Associated types	En route terminal, approach (LNAV) timeout (s)	Approach (LNAV/VNAV, LP, LPV) timeout (s)
PRN mask	31	600	600
Integrity information	32, 34–36, 40	18	12
Clock-ephemeris error corrections and covariance matrix	32	Variable	Variable
Almanacs of SBAS satellite	47	360	360

**Table 3** Main information on B1C messages

Contents	Associated types	En route terminal, approach (LNAV) timeout (s)	Approach (LNAV/VNAV, LP, LPV) timeout (s)
PRN mask	1	600	600
Fast corrections	2–5, 24	Variable	Variable
GEO navigation data	9	360	240
Timing data	12	86,400	86,400
Almanac data	17	–	–
Long-term corrections	24, 25	360	240
Ionospheric masks	18	1200	1200
Ionospheric corrections	26	600	600
Service level	27	86,400	86,400
Clock-ephemeris covariance matrix	28	360	240

$$dP_{r,i}^{(s)} = \mathbf{l}_r^{(s)} \mathbf{x} + t_r - t^{(s)} + \xi_{r,IF} - \xi_{IF}^{(s)} + \Gamma_r^{(s)} T_r^z + \varepsilon_{r,IF}^{(s)} \quad (3)$$

$$\begin{aligned} d\phi_{r,i}^{(s)} = & \mathbf{l}_r^{(s)} \mathbf{x} + t_r - t^{(s)} + \zeta_{r,IF} - \zeta_{IF}^{(s)} \\ & + \Gamma_r^{(s)} T_r^z + N_{r,IF}^{(s)} + \epsilon_{r,IF}^{(s)} \end{aligned} \quad (4)$$

where  $dP_{r,i}^{(s)}$  and  $d\phi_{r,i}^{(s)}$  denote the code and phase observations on frequency  $i$  ( $i = 1$  or  $2$ ) from receiver  $r$  to satellite  $s$ , respectively;  $dP_{r,IF}^{(s)}$  and  $d\phi_{r,IF}^{(s)}$  the code and phase IF combination observations, respectively;  $\mathbf{l}_r^{(s)}$  the unit vector from the receiver to satellite;  $\mathbf{x}$  the vector of receiver coordinates;  $t_r$  and  $t^{(s)}$  the receiver and satellite clock offsets, respectively;  $\xi_r$  and  $\xi^{(s)}$  the receiver and satellite code hardware delays, respectively;  $\zeta_r$  and  $\zeta^{(s)}$  the receiver and satellite phase hardware delays, respectively;  $\Gamma_r^{(s)}$  and  $T_r^z$  the tropospheric mapping function and zenith tropospheric delays, respectively;  $I_{r,i}^{(s)}$  the slant ionospheric delay;  $N_r^{(s)}$  the ambiguity parameter;  $\varepsilon_r^{(s)}$  and  $\epsilon_r^{(s)}$  the code and phase observation noise, respectively.

As aforementioned, satellite orbit and clock errors can be mitigated by B2b, B2a, B1C, and broadcast ephemeris messages. Ionospheric delays can be mitigated by B1C or broadcast ephemeris messages. DCB, namely satellite code hardware delay, can be mitigated by B2b messages. For the phase hardware delays, it will be absorbed by the ambiguity parameter. Similarly, the code hardware delays of the receiver will be absorbed by the receiver clock offset. Combining B2b, B2a, and B1C services, an InRPPP system is proposed and the relevant observation equations can be written as

$$\begin{pmatrix} \mathbf{P}_{r,i}^{\text{B2b/B2a/B1C/BRDC}} \\ \boldsymbol{\phi}_{r,i}^{\text{B2b/B2a/B1C/BRDC}} \\ \mathbf{P}_{r,IF}^{\text{B2b/B2a/BRDC}} \\ \boldsymbol{\phi}_{r,IF}^{\text{B2b/B2a/BRDC}} \end{pmatrix} = \begin{pmatrix} \mathbf{G}_n \ \mathbf{e}_n \ \mathbf{0} \ \boldsymbol{\Gamma}_n \ \mathbf{0} \ \mathbf{0} \\ \mathbf{G}_n \ \mathbf{e}_n \ \mathbf{0} \ \boldsymbol{\Gamma}_n \ \mathbf{I}_n \ \mathbf{0} \\ \mathbf{G}_m \ \mathbf{0} \ \mathbf{e}_m \ \boldsymbol{\Gamma}_m \ \mathbf{0} \ \mathbf{0} \\ \mathbf{G}_m \ \mathbf{0} \ \mathbf{e}_m \ \boldsymbol{\Gamma}_m \ \mathbf{0} \ \mathbf{I}_m \end{pmatrix} \begin{pmatrix} \mathbf{x} \\ \tilde{t}_{r,i} \\ \tilde{t}_{r,IF} \\ T_r^z \\ \tilde{N}_{r,i} \\ \tilde{N}_{r,IF} \end{pmatrix} + \begin{pmatrix} \boldsymbol{\varepsilon}_i \\ \boldsymbol{\epsilon}_i \\ \boldsymbol{\varepsilon}_{IF} \\ \boldsymbol{\epsilon}_{IF} \end{pmatrix} \quad (5)$$

with equivalent clock offsets  $\tilde{t}_{r,i} = t_r + \xi_{r,i}$ ,  $\tilde{t}_{r,IF} = t_r + \xi_{r,IF}$ , equivalent ambiguity parameters  $\tilde{N}_{r,i}^{(s)} = N_{r,i}^{(s)} + \zeta_{r,i} - \zeta_i^{(s)} - \xi_i^{(s)} - \xi_{r,i}$ ,  $\tilde{N}_{r,IF}^{(s)} = N_{r,IF}^{(s)} + \zeta_{r,IF} - \zeta_{IF}^{(s)} + \xi_{IF}^{(s)} - \xi_{r,IF}$ , where  $\mathbf{P}_{r,i} = (dP_{r,i}^{(1)}, \dots, dP_{r,i}^{(n)})^T$  and  $\boldsymbol{\phi}_{r,i} = (d\phi_{r,i}^{(1)}, \dots, d\phi_{r,i}^{(n)})^T$  denote the SF code and phase observations with  $n$  satellites, respectively;  $\mathbf{P}_{r,IF} = (dP_{r,IF}^{(1)}, \dots, dP_{r,IF}^{(m)})^T$  and  $\boldsymbol{\phi}_{r,IF} = (d\phi_{r,IF}^{(1)}, \dots, d\phi_{r,IF}^{(m)})^T$  the IF code and phase observations with  $m$  satellites, respectively; the superscripts B2b, B2a, B1C, and BRDC the B2b, B2a, B1C, and broadcast ephemeris messages, respectively;  $\mathbf{G}_j = (\mathbf{l}_r^{(1)}, \dots, \mathbf{l}_r^{(j)})$  ( $j = n, m$ ) the design matrix of  $\mathbf{x}$ ;  $\boldsymbol{\Gamma}_j = (\Gamma_r^{(1)}, \dots, \Gamma_r^{(j)})^T$  the design matrix of  $T_r^z$ ;  $\boldsymbol{\varepsilon}_i = (\varepsilon_{r,i}^{(1)}, \dots, \varepsilon_{r,i}^{(n)})^T$  and  $\boldsymbol{\epsilon}_i = (\epsilon_{r,i}^{(1)}, \dots, \epsilon_{r,i}^{(n)})^T$  the observation noise of SF code and phase observations, respectively;  $\boldsymbol{\varepsilon}_{IF} = (\varepsilon_{r,IF}^{(1)}, \dots, \varepsilon_{r,IF}^{(m)})^T$  and  $\boldsymbol{\epsilon}_{IF} = (\epsilon_{r,IF}^{(1)}, \dots, \epsilon_{r,IF}^{(m)})^T$  the observation noise of IF code and phase observations, respectively. The symbol  $\mathbf{e}_j$  denotes a column vector of  $j$ -dimension with value one; symbol  $\mathbf{I}_j$  the  $j$ -dimension identity matrix. If

there are other satellite systems or signals, new corresponding clock offsets need to be estimated separately since there exist inter-system biases, DCBs, and even inter-frequency clock biases.

As to stochastic model, we employ realistic weighting function to characterize the precision of observations and messages, which can be written as

$$\left\{ \begin{array}{l} (\sigma_{P_i})^2 = (\sigma_P)^2 + \left( \sigma_{OC}^{B2b/B2a/BRDC} \right)^2 + \left( \sigma_{ION}^{B1C/BRDC} \right)^2 \\ (\sigma_{\phi_i})^2 = (\sigma_\phi)^2 + \left( \sigma_{OC}^{B2b/B2a/BRDC} \right)^2 + \left( \sigma_{ION}^{B1C/BRDC} \right)^2 \\ (\sigma_{P_{IF}})^2 = (\alpha_{IF})^2 \cdot \left( (\sigma_P)^2 + \left( \sigma_{OC}^{B2b/B2a/BRDC} \right)^2 \right) \\ (\sigma_{\phi_{IF}})^2 = (\alpha_{IF})^2 \cdot \left( (\sigma_\phi)^2 + \left( \sigma_{OC}^{B2b/B2a/BRDC} \right)^2 \right) \end{array} \right. \quad (6)$$

where  $\sigma_{P_i}$  and  $\sigma_{\phi_i}$  denote the Standard Deviations (STDs) of SF code and phase observations, respectively;  $\sigma_{P_{IF}}$  and  $\sigma_{\phi_{IF}}$  the STDs of DF IF code and phase observations, respectively;  $\sigma_P$  and  $\sigma_\phi$  the STDs of observations mainly considering the noise which is the function of elevation, respectively;  $\sigma_{OC}$  the STD of satellite orbit and clock corrections;  $\sigma_{ION}$  the STD of ionospheric corrections;  $\alpha_{IF}$  the amplification factor of the IF combination. Based on this, variance component estimation can also be utilized to optimize the variance factors (Xu et al., 2006; Xu et al., 2014).

The flowchart of the InRPPP system is illustrated in Fig. 2. First, special format broadcast ephemeris, observations, and the latest B1C, B2a, and B2b messages are collected. Subsequently, the latest messages are resiliently

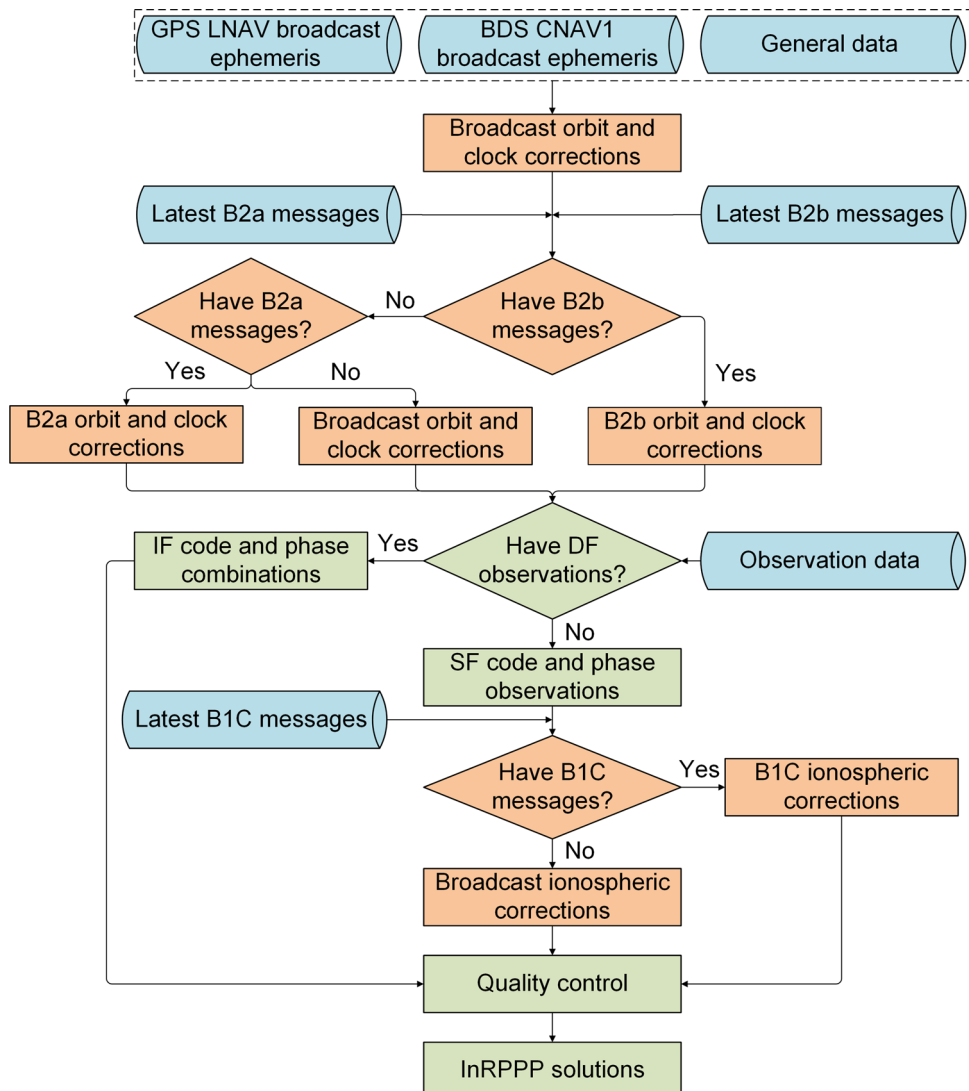


**Fig. 2** Flowchart of the InRPPP system

used to better correct satellite orbit, clock, and ionospheric errors. Previous research has demonstrated that B2b orbit and clock corrections offer the highest accuracy, followed by B2a corrections, while broadcast ephemeris and B1C corrections are equally accurate (Wu et al., 2024). B1C ionospheric corrections are notably more precise than the Klobuchar model (Nie et al., 2019). Thus, if the B2b messages are available and successfully matched, these messages are given priority for use; otherwise, B2a messages are used. If B2a messages are not available, broadcast ephemeris is used. For DF IF combination observations, namely  $P_{r,\text{IF}}$  and  $\phi_{r,\text{IF}}$  in (5), the corrections are applied only for satellite orbit errors and clock offsets using external messages. However, for SF observations, namely  $P_{r,i}$  and  $\phi_{r,i}$  in (5), an additional correction for ionospheric delays is required. First, B1C ionospheric corrections are applied. If B1C messages are not available, the Klobuchar model or another empirical model is employed to mitigate ionospheric delays. It is noteworthy that due to the relatively low accuracy of B1C ionospheric corrections and the Klobuchar model, the residual ionospheric errors will still remain, which may lead to a bias in the SF mathematical model. Therefore, compared to the DF IF combination observations, the SF observations are generally assigned with lower weights, as indicated by (6), especially the SF measurements with the Klobuchar model. Finally, based on the quality control method and extended Kalman filter, we can get InRPPP solutions (Teunissen, 2018; Zhang et al., 2024).

#### Validation of InRPPP system with B2b, B2a, and B1C services

To further demonstrate the viability of the InRPPP system, we systematically evaluate the positioning accuracy with B2b, B2a, B1C, and broadcast ephemeris messages used in PPP mode. This evaluation utilizes the data at station WUH2, covering Day of Year (DOY) 251–253 in 2023. Table 4 describes different solution

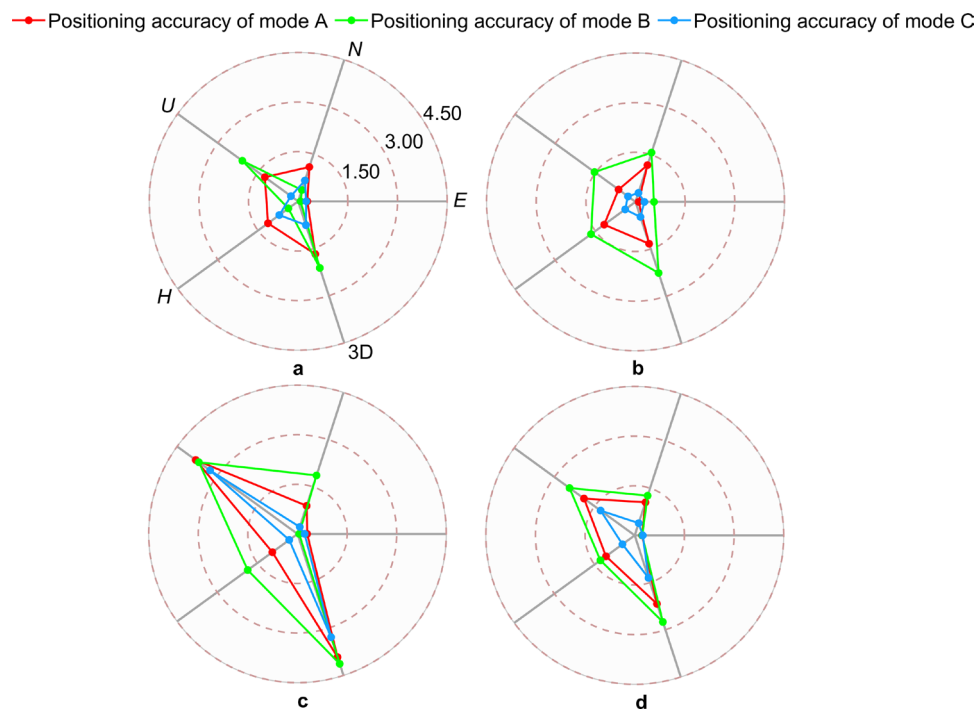
modes for evaluation. To mitigate the influence of initial convergence on positioning accuracy, only the post-convergence data (e.g., after four hours of observations in this study) is used for accuracy assessment.

Figure 3 shows the positioning accuracy for modes A, B, and C on DOY **a** 251, **b** 252, **c** 253, and **d** average. Compared with modes B and C, mode C exhibits better accuracy due to the use of more precise B1C ionospheric corrections. This suggests that B1C ionospheric corrections are of greater importance for PPP mode compared to those with broadcast ephemeris. Unfortunately, comparing to mode A, the positioning accuracy of mode B deteriorates when using B1C orbit and clock corrections. This decline is related to the limited availability of B1C messages, which reduces the number of satellites with B1C messages, thereby degrading the positioning accuracy. Meanwhile, some studies suggest that the accuracy of B1C orbit and clock corrections is comparable to the accuracy of broadcast ephemeris (Hu et al., 2023). Therefore, compared to B1C messages, broadcast ephemeris has greater value for satellite orbits and clocks.

Figure 4 shows the positioning accuracy for modes D, E, and F on DOY **a** 251, **b** 252, **c** 253, and **d** average. Mode F demonstrates the highest performance, followed by mode E. This trend correlates with the precision levels of the orbit and clock corrections, where B2b provides the highest accuracy, B2a follows, and broadcast ephemeris shows the lowest precision. Previous research reported similar results (Bahrami et al., 2016; Nie et al., 2019; Hu et al., 2023). From the above, for orbit errors and clock offsets, B2b messages should have priority, followed by B2a, with broadcast ephemeris as the least option. For ionospheric delays, the B1C ionospheric corrections are used first, followed by the broadcast ephemeris. In this way, the InRPPP system with B2b, B2a, and B1C messages using mixed SF and DF positioning mode is reasonable, confirming the effectiveness of all message types within the system.

**Table 4** Different solution modes for evaluation

Abbreviation	Mode	Observations	Orbit and clock corrections	Ionospheric corrections
A	SF-PPPBRC	GPS L1	Broadcast ephemeris	Broadcast ephemeris
B	SF-PPPB1C1	GPS L1	B1C messages	Broadcast ephemeris
C	SF-PPPB1C2	GPS L1	B1C messages	B1C messages
D	DF-PPPBRC	GPS L1/L5 BDS B1C/B2a	Broadcast ephemeris	IF combination
E	DF-PPPB2a	GPS L1/L5 BDS B1C/B2a	B2a messages	IF combination
F	DF-PPPB2b	GPS L1/L5 BDS B1C/B2a	B2b messages	IF combination



**Fig. 3** Positioning accuracy of modes A, B, and C on DOY 251 (a), 252 (b), 253 (c), and average (d)

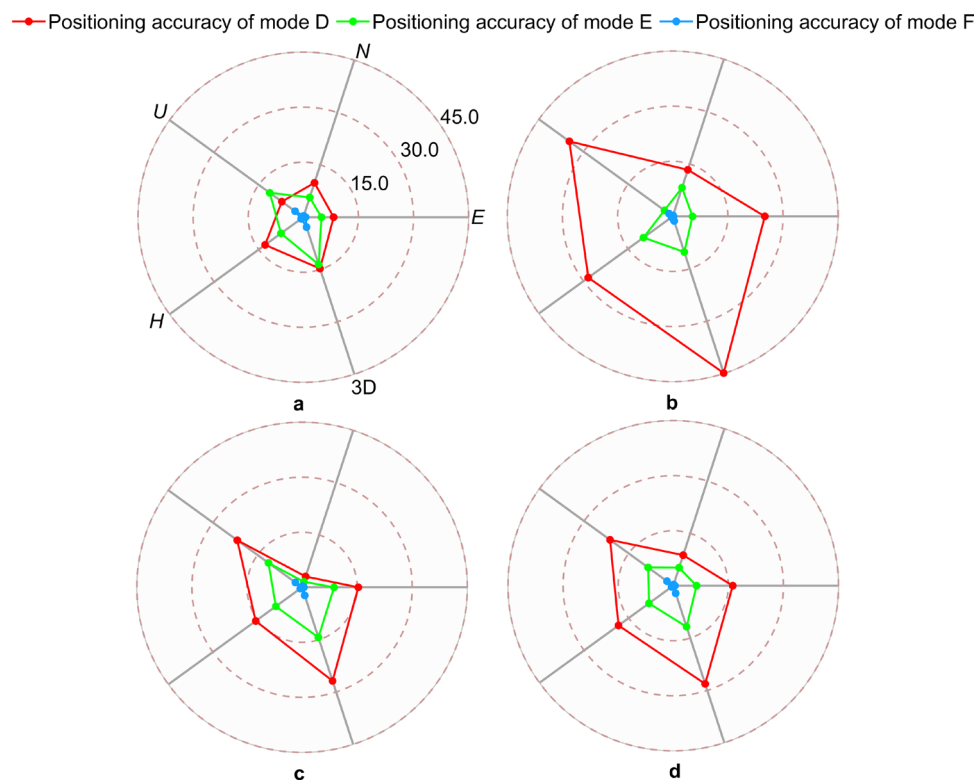


**Fig. 4** Positioning accuracy of modes D, E, and F on DOY 251 (a), 252 (b), 253 (c), and average (d)



**Fig. 5** Scenes of the static experiment. The left and right panels denote the west and south sides of the station

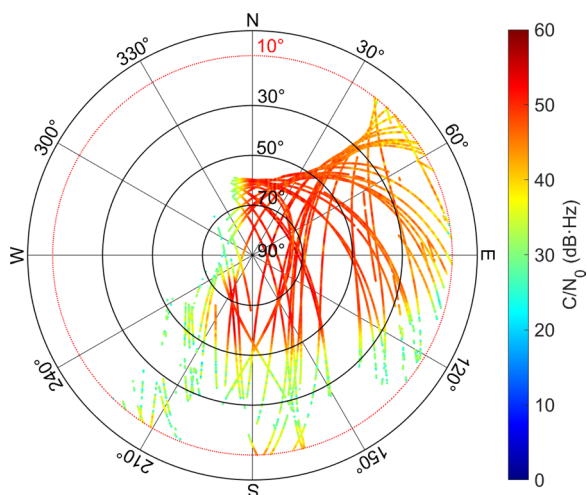


**Fig. 6** Sky plot with  $C/N_0$  information in the static experiment

### Measurement campaigns

To evaluate the property of the InRPPP system, both static and kinematic experiments are conducted under complex conditions. The details of these experiments are given and the corresponding solution modes are also illustrated.

#### Static experiment

In this study, a static experiment in the high-occlusion environments was designed. The dataset was collected at Hohai University, China, on DOY 251 in 2023. The reference coordinates were calculated with the post-processed PPP mode using precise products. Figure 5 shows the scenes of the static experiment and Fig. 6 shows the sky plot with  $C/N_0$  information. From Fig. 5, there is high-occlusion to the west and

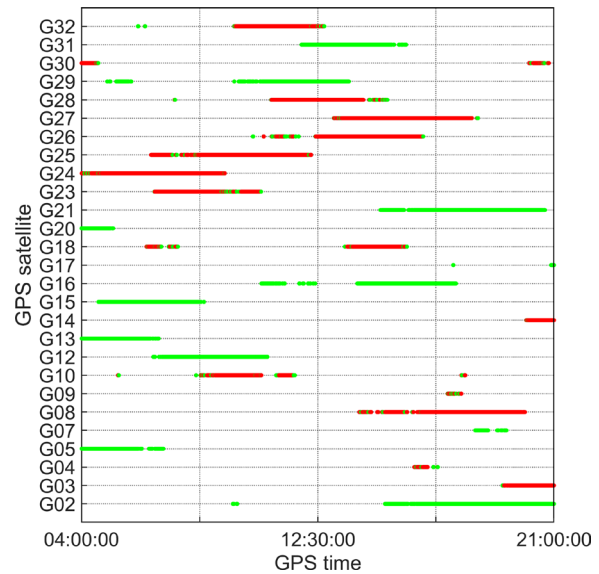


**Fig. 7** Visibility of GPS satellites with frequency information in the static experiment. The green and red colors denote the satellite with SF and DF observations, respectively

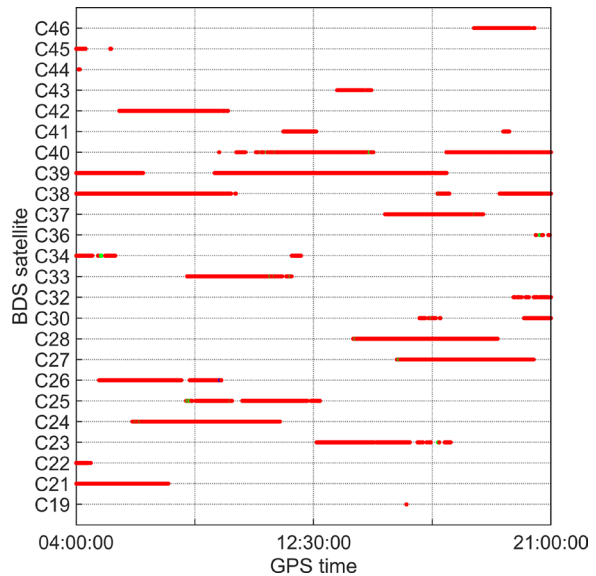


**Fig. 8** Visibility of BDS satellites with frequency information in the static experiment. The green and red colors denote the satellite with SF and DF observations, respectively

south of the station, which hinders the GNSS signal propagation, especially from the west direction. This obstruction results in particularly low  $C/N_0$  values in the west direction, even at high elevations. Given the limitations of the B2a service, we prefer to use the GPS L1 and L5, BDS B1C and B2a signals to highlight the performance of the InRPPP system. Figure 7 and

**Table 5** Processing strategies of PPP

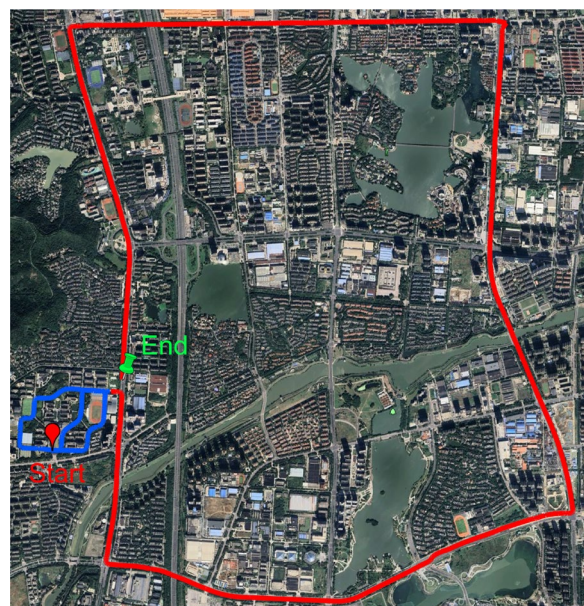
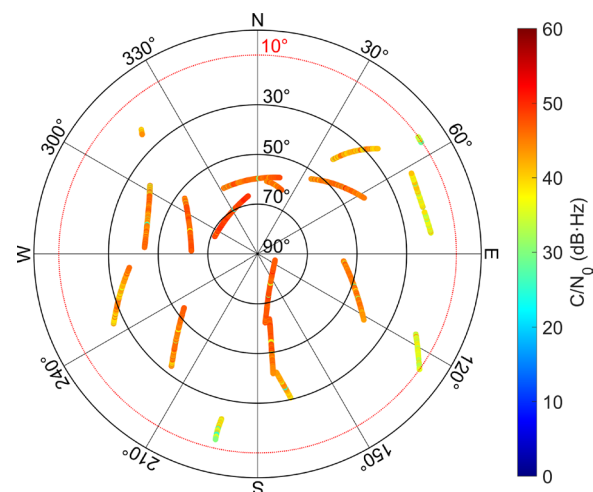
Item	Strategy
Sampling rate	1 s
Estimator	Extended Kalman filter
Cut-off elevation	10°
Tropospheric delay	Estimated as random walk process
Receiver position	Estimated as constants at each epoch
Receiver clock offset	Estimated as white noise at each epoch
Ambiguity	Estimated as a constant float value each arc

**Table 6** Different solution modes

Mode	Explanation
PPP-B1C	Use B1C messages and SF observations
PPP-B2a	Use B2a messages and IF combination observations
PPP-B2b	Use B2b messages and IF combination observations
InRPPP	Use B2b, B2a, B1C, and broadcast ephemeris messages and mixed SF and DF IF combination observations

8 present the frequency information of GPS and BDS satellites, respectively. Due to the high-occlusion environments around the station, only a few satellites with DF observations can be observed at each epoch. Also, since there are very few GPS satellites broadcasting L5 signal, most GPS satellites have only SF frequency. Due to the high-occlusion environments, the GPS satellites often have signal interruptions. Compared to the GPS satellites, the B1C and B2a signals exhibit strong stability, with signal interruptions occurring only at a few epochs.

Various solution modes were carried out using different modes to analyze the property of the InRPPP system. Table 5 shows the common processing strategies of PPP. In addition to the traditional PPP-B2b mode using B2b messages, we applied B1C and B2a messages to PPP mode, namely PPP-B1C and PPP-B2a modes, respectively. Table 6 describes different modes. Specifically, they are PPP-B1C mode using B1C orbit, clock, and ionospheric corrections and GPS L1 SF observations; PPP-B2a mode using B2a orbit and clock corrections and GPS L1/L5 and BDS B1C/B2a IF combination observations; PPP-B2b mode using B2b orbit and clock corrections and GPS L1/L5 and BDS B1C/B2a IF combination observations; and InRPPP mode using InRPPP system, where B2b, B2a, B1C, and broadcast ephemeris messages are all resiliently utilized.

**Fig. 9** Trajectory of the kinematic experiment. The Start and End markers denote the start and end points, respectively**Fig. 10** Sky plot with  $C/N_0$  information in the kinematic experiment

### Vehicle kinematic experiment

A vehicle kinematic experiment was also conducted on DOY 251 in 2023, from GPS time 02:30:35 to 03:17:50 in Nanjing, China. Figure 9 shows the trajectory of the kinematic experiment. The kinematic experiment was divided into two parts. First, from GPS time 02:30:35 to 02:38:30, the vehicle moved at low speed in canopy environments. Second, from GPS time 02:38:31 to 03:17:50, the vehicle moved at high speed in canyon environments. The geodetic receiver was equipped with high-precision GNSS/Inertial Navigation System (INS), which can provide reliable reference coordinates. Figure 10 shows the

sky plot with  $C/N_0$  information. Different from the static experiment, short observation periods and vehicle environments often result in reduced visibility windows for each satellite and lower  $C/N_0$  values, indicating degraded satellite signal quality in vehicle environments. Moreover, due to the unstable environments, the  $C/N_0$  values present variations regardless of the elevation angle. Fig. 11 shows satellite visibility with frequency information. Similarly, due to the vehicle environments, the signals exhibit more frequent interruptions regardless of GPS or BDS satellites compared to the static experiment. Similarly, the four modes, namely PPP-B1C, PPP-B2a, PPP-B2b, and InRPPP modes are all compared and the descriptions are presented in Table 6.

## Results and discussion

In this section, two typical experiments were conducted to evaluate the performance of the InRPPP system. The first is the static experiment conducted in the high-occlusion environments, and the second is the kinematic experiment in the vehicle environments.

### Static experiment

To assess the performance of the InRPPP system, the results for the four modes, namely PPP-B1C, PPP-B2a, PPP-B2b, and InRPPP modes, are analyzed and compared in terms of visible satellite numbers, PDOP values, accuracy, and convergence time. Specifically, the accuracy is evaluated using the Root-Mean-Square (RMS) errors of positioning results compared to reference

coordinates which are obtained using the PPP mode with precise products. To assess convergence time, we defined different convergence criteria for the static experiment based on the positioning biases in the East ( $E$ ), North ( $N$ ), and Up ( $U$ ) directions, with different thresholds for each condition. Considering the positioning accuracy of PPP-B2b service and high-occlusion environments, for Condition A the thresholds in the  $E/N/U$  directions are 0.60/0.40/0.80 m, respectively; Condition B 0.30/0.20/0.40 m; Condition C 0.25/0.15/0.30 m; and Condition D 0.20/0.10/0.25 m. For each condition, the positioning biases must remain below the threshold for a minimum of 200 epochs.

Figure 12 shows the visible satellite numbers and PDOP values in the static experiment. Obviously, the visible satellite numbers in the InRPPP mode are the largest. The resilient utilization of B2b, B2a, B1C, and broadcast ephemeris messages can significantly increase the visible satellite numbers, indicating that the InRPPP system effectively leverages all available observations and external messages, thereby enhancing positioning availability and accuracy. As the B1C service can only augment the GPS L1 frequency, the PPP-B1C mode cannot have solutions in certain periods due to the visible satellite numbers and message availability limitations in high-occlusion environments. Moreover, the B2b service augments all GPS and BDS satellites, while the B2a service only augments the satellites broadcasting L1/L5 or B1C/B2a signals. Thus, although we utilize L1/L5 and B1C/B2a signals, the satellite numbers in the PPP-B2b mode are still larger than those in the PPP-B2a mode. Similarly, the PDOP values in InRPPP mode are the smallest and the most stable among the four modes. There are frequent and large fluctuations, especially in PPP-B2a mode, due to the fact that the B2a service can only augment limited

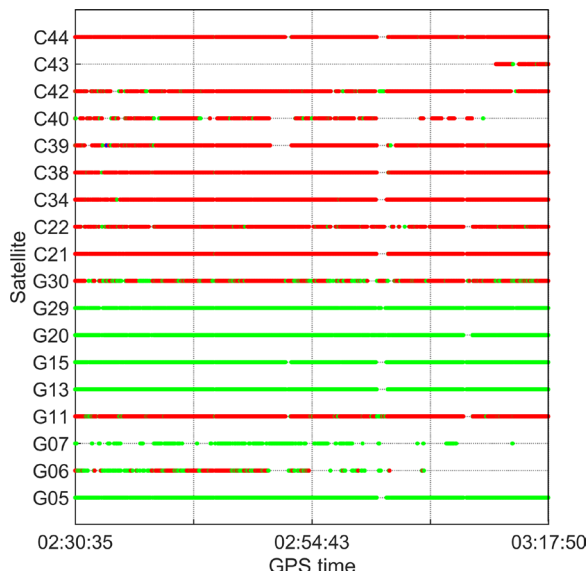


**Fig. 11** Satellite visibility with frequency information in the kinematic experiment. The green and red colors denote the satellite with SF and DF observations, respectively

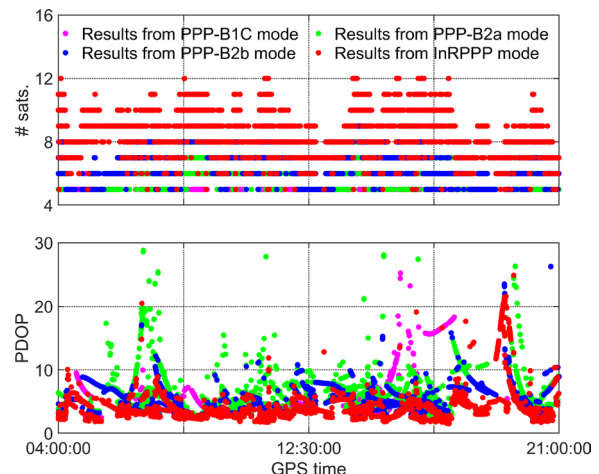


**Fig. 12** Satellite numbers and PDOP values in the static experiment

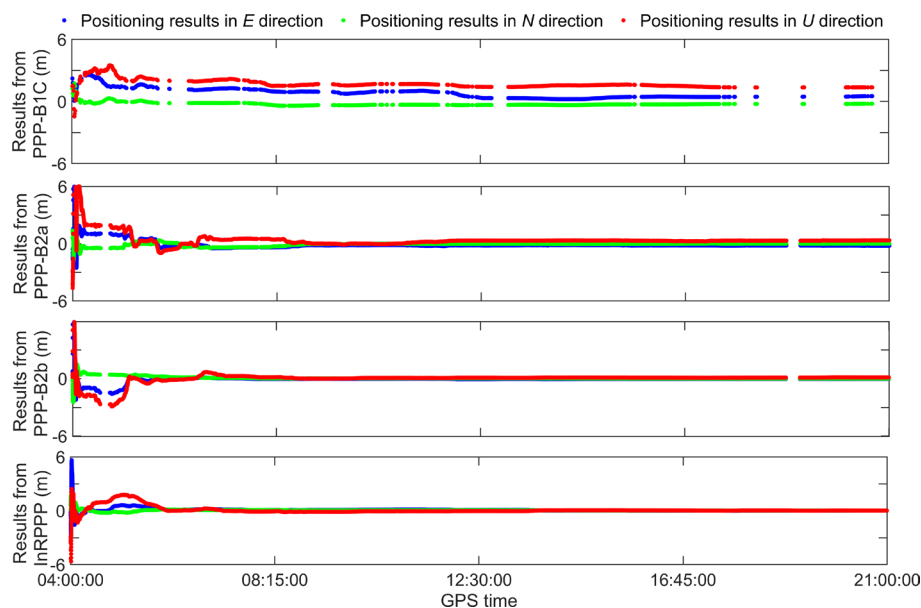
satellites. Around GPS time 19:30:00, the PDOP values of PPP-B2a and PPP-B2b modes are very large because some satellites are blocked and then the geometry deteriorates. In contrast, the InRPPP mode can effectively suppress these fluctuations and reduce PDOP values by combining B2b, B2a, B1C, and broadcast ephemeris messages.

Figure 13 presents the static positioning results. Considering the PPP-B1C, PPP-B2a, and PPP-B2b modes, we can see that in different periods there are no solutions, especially the PPP-B1C mode, due to the limited satellite numbers and message availability limitations in the high-occlusion environments. While the InRPPP mode has solutions during these periods due to the resilient utilization of all external messages. This fact indicates that the InRPPP mode can effectively improve the continuity and availability of solutions. Furthermore, we can see that the curve of positioning results in the *E* direction exhibits significantly larger fluctuations compared to the *N* direction. This discrepancy is due to the high-occlusion in the west direction, which severely hinders signal reception and consequently affects the accuracy in the *E* direction. After convergence, the PPP-B1C mode exhibits a large bias of about 1.1 m and 1.8 m, respectively, in the *E* and *U* directions, which can be attributed to the lower precision of the B1C messages. Due to the comprehensive and resilient utilization of B2b, B2a, B1C, and broadcast ephemeris messages, the fluctuations of the positioning error curves for the InRPPP mode are minimized in all directions compared to the PPP-B2a and PPP-B2b

modes. This indicates that the InRPPP mode performs the best.

To better demonstrate the superiority of the InRPPP system, Figs. 14 and 15 present the message utilization of GPS and BDS satellites, respectively. It is observed that in the InRPPP mode, all external messages can be resiliently utilized. Taking GPS satellites as an example, since only a few satellites broadcast the L5 frequency, the phenomenon of mixed SF and DF observations is more pronounced compared to BDS satellites. On the one hand, for the SF observations, the inclusion of B1C messages effectively mitigates ionospheric delays. The addition of SF observations significantly increases the number of available satellites. On the other hand, since the reception of B2b messages is limited, the incorporation of B2a messages helps better correct the orbit and clock errors of satellites lacking B2b messages, further enhancing the number of available satellites. Thus, in this way, all external messages can be effectively utilized, which enhances the positioning performance of the InRPPP system.

To quantitatively analyze the distinction among the four modes, Table 7 presents the static positioning performance for different modes and the average convergence time for Conditions A to D mentioned above. The overall RMS values of 3D positions for the PPP-B1C, PPP-B2a, and PPP-B2b modes are 2.01 m, 1.14 m, and 0.91 m, respectively. Compared to the PPP-B1C, PPP-B2a, and PPP-B2b modes, the 3D RMS values for the InRPPP mode are improved by 75.6%, 57.0%, and 46.2%, respectively. As expected, the InRPPP mode has the best



**Fig. 13** Static positioning results. The panels arranged from top to bottom denote the results of PPP-B1C, PPP-B2a, PPP-B2b, and InRPPP modes, respectively.

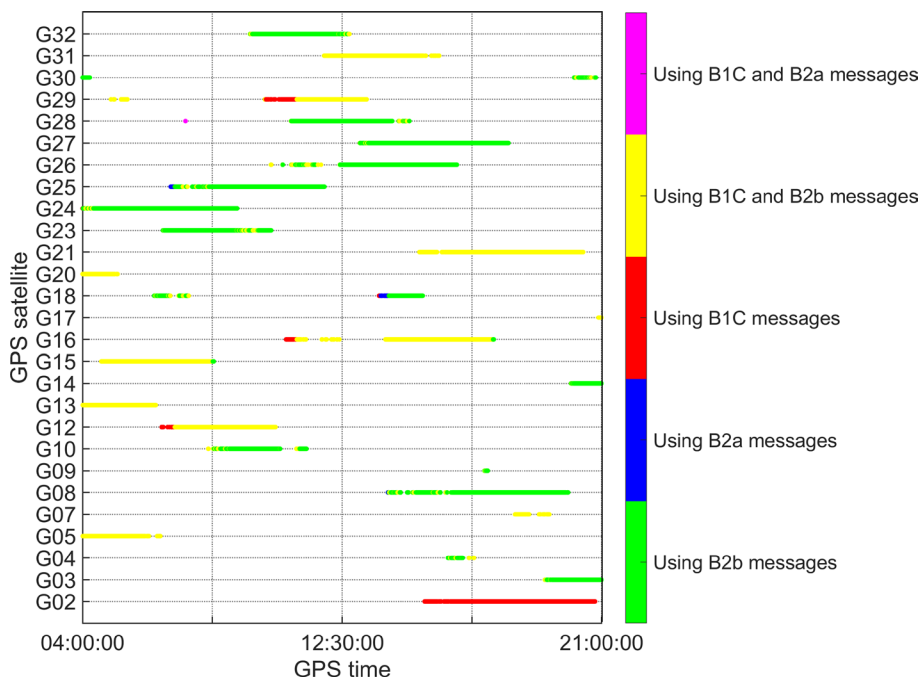


**Fig. 14** Message utilization of GPS satellites in the static experiment

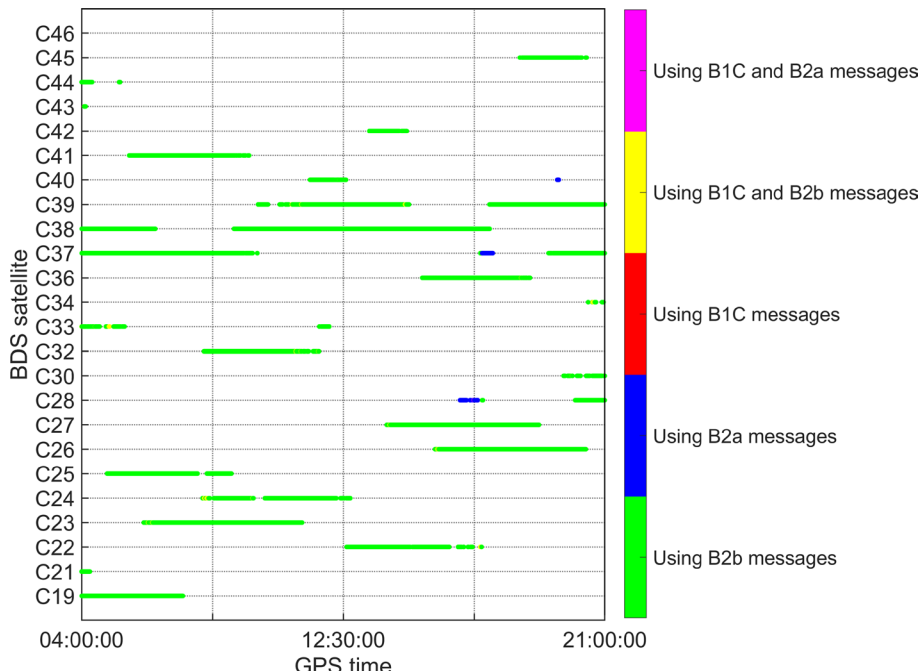


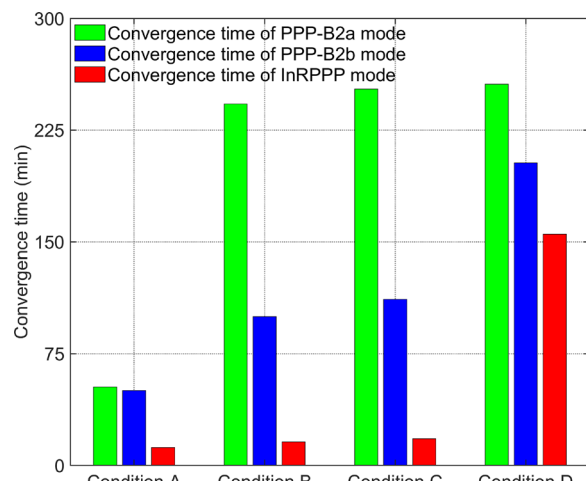
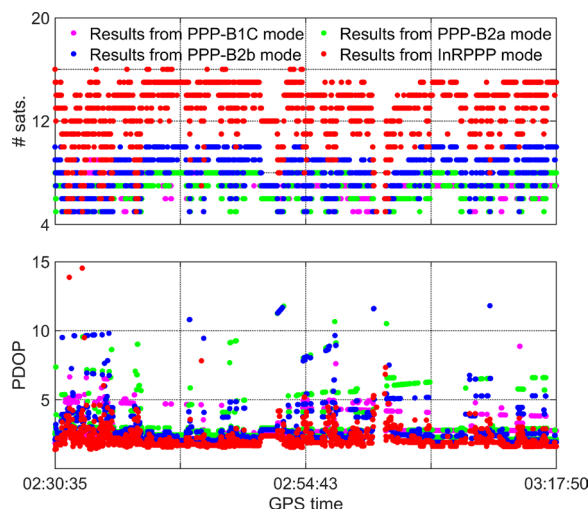
**Fig. 15** Message utilization of BDS satellites in the static experiment

positioning accuracy. In conclusion, the InRPPP mode not only has the largest number of visible satellite but also has the smallest PDOP values, thereby achieving superior positioning accuracy and improving the continuity and availability of solutions.

Then, the convergence time using the InRPPP mode in the static experiment is analyzed. It is worth noting that the PPP-B1C mode fails to meet the convergence criteria due to the large bias mentioned above, and thus, its convergence time is not calculated. Figure 16 presents

**Table 7** Static positioning performance with different modes

Mode	RMS in different directions (m)				Mean convergence time (min)
	Results in E direction	Results in N direction	Results in U direction	Results in three-direction	
PPP-B1C	0.93	0.31	1.76	2.01	–
PPP-B2a	0.52	0.18	1.00	1.14	200.97
PPP-B2b	0.51	0.17	0.74	0.91	116.27
InRPPP	0.24	0.09	0.42	0.49	50.25

**Fig. 16** Convergence time of different modes and conditions in the static experiment**Fig. 17** Satellite numbers and PDOP values in the kinematic experiment

the convergence time for different modes and conditions in the static experiment. Due to the use of observations in high-occlusion environments, the convergence time is relatively slower regardless of the solution mode. It is observed that as the convergence criteria become more stringent, the required convergence time increases accordingly, especially for the PPP-B2a mode. For different convergence criteria, the convergence time of the InRPPP mode consistently outperforms both the PPP-B2a and PPP-B2b modes, indicating the shortest convergence time. Taking Condition B as an example, the convergence time for InRPPP mode can be improved by 93.5% and 84.1% compared to the PPP-B2a and PPP-B2b modes, respectively. As shown in Table 7, considering the four convergency conditions, the convergence time for the InRPPP mode can be improved by approximately 75.0% and 56.8%, respectively, compared to the PPP-B2a and PPP-B2b modes. In short, the InRPPP mode has the shortest convergence time, followed by the PPP-B2b mode. From the above, the InRPPP mode presents the best performance, which not only has the largest satellite numbers and the smallest PDOP values but also has the

best positioning accuracy and the shortest convergence time.

#### Kinematic experiment

In addition to the static experiment, a vehicle kinematic experiment was performed to further validate the superiority of the InRPPP mode. Figure 17 displays the visible satellite numbers and the PDOP values. Due to the different conditions, the first part in canopy environment exhibits smaller satellite numbers and higher PDOP values with significant fluctuations compared to the second part in canyon environment. Similar to the static experiment, the visible satellite numbers for the InRPPP mode are the largest. Consequently, the PDOP values are the smallest and the most stable among the four modes. It is easy to understand that due to the resilient utilization of the B2b, B2a, B1C, and broadcast ephemeris messages, the InRPPP mode can optimally use all observations and messages, thereby effectively increasing the satellite numbers. Furthermore, the sudden fluctuations in PDOP values suggest the frequent changes in the satellite geometry during the experiment, indicating an unstable

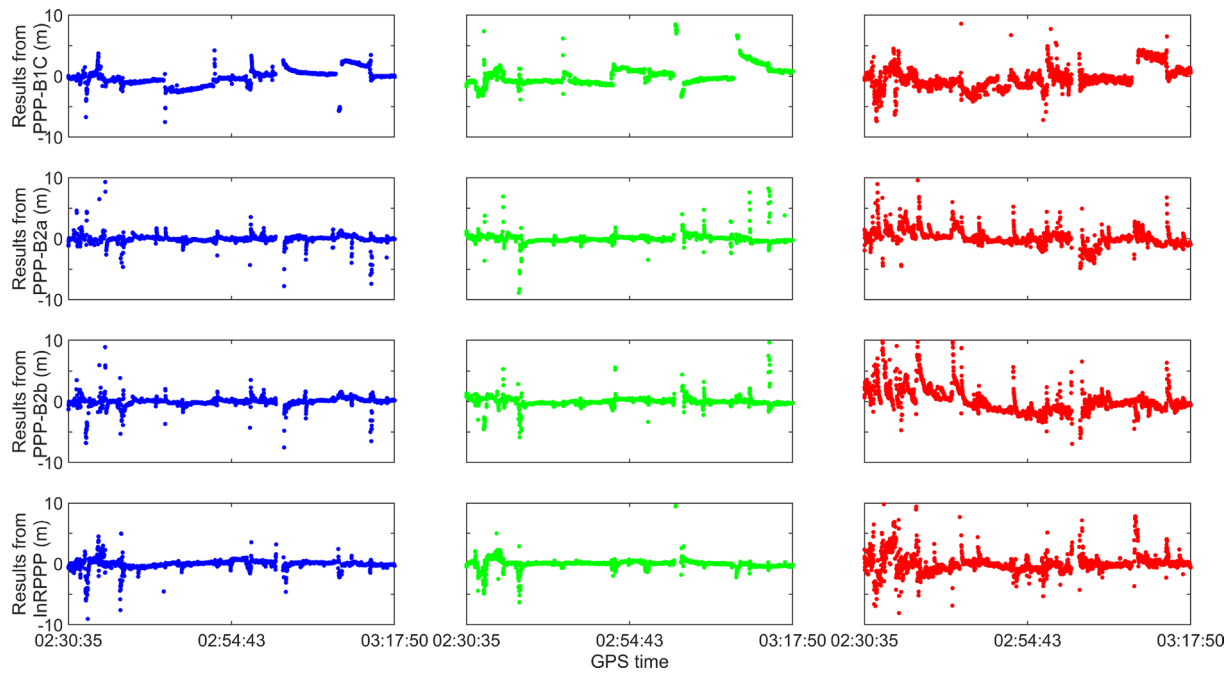


**Fig. 18** Kinematic positioning results. The panels arranged from top to bottom denote the results of PPP-B1C, PPP-B2a, PPP-B2b, and InRPPP modes, respectively. The results filled with blue, green, and red colors denote those in the *E*, *N*, and *U* directions, respectively

environment that may disrupt GNSS signal propagation and lead to frequent signal interruptions.

Moreover, the kinematic positioning results are shown in Fig. 18. Similar to the static experiment, the PPP-B1C mode also has a large bias due to the relatively low precision of the B1C messages. Furthermore, the PPP-B1C mode exhibits frequent reconvergence phenomena due to the environment and limited message availability. When the vehicle entered complex environments, frequent and significant jumps are observed for the PPP-B2a, PPP-B2b, and InRPPP modes, especially in the *U* direction. This instability is primarily due to unstable environments, such as tree-shaded environments, and vehicle environments. These conditions lead to frequent satellite signal obstructions and interruptions, complicating ambiguity resolution and causing significant errors. In some periods, the phenomenon that the InRPPP and PPP-B2b modes have larger jumps than the PPP-B2a mode can be attributed to the different availability. From Fig. 17, the visible satellite numbers for the InRPPP and PPP-B2b modes are larger than the PPP-B2a modes, which means that the InRPPP and PPP-B2b modes have higher availability and solutions in complex environments, while the PPP-B2b cannot have solutions. However, due to the existence of gross errors and multipath effects, these solutions are of poor quality and present as large jumps. Although the jumps for InRPPP and PPP-B2b modes are occasionally larger than those for PPP-B2a

mode, the overall performance for PPP-B2b and InRPPP modes remains superior. Consistent with the previous paragraph, the first part in canopy environment has more jumps. At GPS time 02:33:00, the vehicle entered a tree-shaded environment where only very few satellites were observed. During this period, the PPP-B2a solutions were unavailable and exhibited significant jumps, as did in the PPP-B2b mode. In contrast, the InRPPP mode can effectively suppress the jumps and increase the availability and stability of the solutions due to the resilient utilization of the B2b, B2a, B1C, and broadcast ephemeris messages.

Figure 19 presents the message utilization of GPS and BDS satellites. Similar to the static experiment, the phenomenon of mixed SF and DF observations still exists in the kinematic experiment, and thus the InRPPP system continues to demonstrate its superiority. However, unlike the static experiment, in the kinematic environment, signal interruptions occur frequently due to the uncertainty of the surrounding environment. As a result, issues such as cycle slips and re-convergence are more pronounced, which severely affect the kinematic positioning performance.

Table 8 presents the kinematic positioning accuracy for different modes. Different from the static experiment, the PPP-B2b mode does not show a significant improvement over the PPP-B2a mode, only a 7.3% improvement in the 3D components of position. This can be attributed to the primary difference between

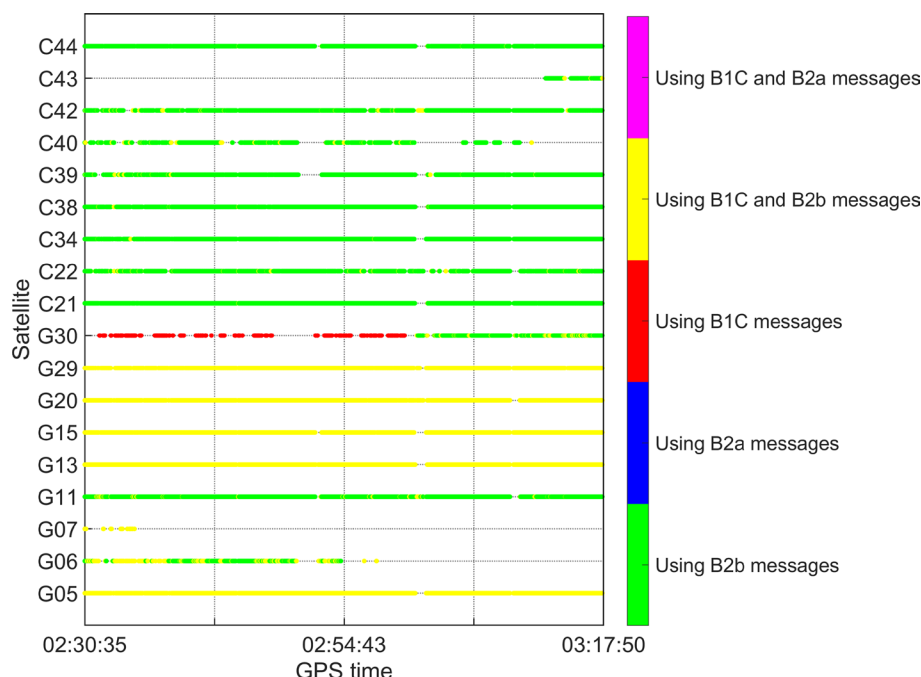


**Fig. 19** Message utilization of GPS and BDS satellites in the kinematic experiment

**Table 8** Kinematic positioning accuracy with different modes

Mode	RMS in different directions (m)			
	Results in E direction	Results in N direction	Results in U direction	Results in three-direction
PPP-B1C	3.43	1.82	3.71	5.37
PPP-B2a	0.76	0.87	3.38	3.57
PPP-B2b	0.86	1.10	3.00	3.31
InRPPP	1.49	0.72	2.00	2.60

B2b and B2a messages, where the precision of orbit and clock corrections is different. However, in the kinematic environment, the precision of orbit and clock corrections are no longer the dominant factors affecting positioning accuracy. Instead, the primary factors influencing positioning accuracy are unresolved ambiguities and multipath effects caused by frequent satellite signal interruptions and complex environments in the experiment. Consistent with the previous paragraph, due to the existence of some larger jumps, the horizontal accuracies for InRPPP and PPP-B2b modes are worse than the PPP-B2a mode, while the 3D accuracies are better than the PPP-B2a mode. As expected, the InRPPP mode can achieve a significant improvement, with 51.6%, 27.2%, and 21.5% improvements in the 3D components of position compared to the PPP-B1C, PPP-B2a, and PPP-B2b modes, respectively. Overall, the InRPPP mode exhibits the best performance in

terms of visible satellite numbers, PDOP values, and positioning accuracy in the kinematic experiment.

In conclusion, the InRPPP system with B2b/B2a/B1C services presents superior performance in both static and kinematic experiments. First, due to the resilient utilization of the B2b, B2a, B1C, and broadcast ephemeris messages, the InRPPP system can fully use all available augmentation messages, thereby improving the continuity and availability of solutions. Second, the integration of the SF observations with B1C ionospheric corrections can effectively increase redundant observations, enhance the robustness of the observation equations, and consequently accelerate convergence. Finally, the satellite orbit and clock errors are corrected by the B2b and B2a services, and the ionospheric delays by the B1C services. In this way, the InRPPP can resiliently utilize all external corrections and observations, increasing the satellite numbers, and thus improving the positioning accuracy.

## Conclusion

In this study, the InRPPP system with B2b/B2a/B1C services is proposed. The primary innovation of the InRPPP system is that it is the first time to utilize the B2b, B2a, B1C, and broadcast ephemeris messages resiliently. Specifically, in the InRPPP system, the satellite orbit and clock errors are corrected by the B2b and B2a services, and the ionospheric delays by the B1C services. To assess the property of the InRPPP system, one static experiment

in the high-occlusion environments and one kinematic experiment in the vehicle environments are carried out.

The primary conclusions are as follows. First, in the static experiment, compared to the PPP-B1C, PPP-B2a, and PPP-B2b modes, the InRPPP system performs the best in terms of visible satellite numbers and PDOP values. Also, the InRPPP mode achieves the highest accuracy and the shortest convergence time. Specifically, the 3D RMS value of the InRPPP mode is 0.49 m, which improves by approximately 75.6%, 57.0%, and 46.2% compared to the PPP-B1C, PPP-B2a and PPP-B2b modes, respectively. For the convergence time, compared to PPP-B2a and PPP-B2b modes, approximately 75.0% and 56.8% improvements are obtained when using the InRPPP mode on the whole. Second, in the kinematic experiment, once again, compared to the PPP-B1C, PPP-B2a, and PPP-B2b modes, the number of satellites is the largest and the PDOP values are the smallest for the InRPPP mode. In addition, in the InRPPP solutions, the jumps are suppressed and the availability and stability are increased. Specifically, 51.6%, 27.2%, and 21.5% improvements are obtained compared to the PPP-B1C, PPP-B2a, and PPP-B2b modes, respectively.

In conclusion, the InRPPP system with B2b/B2a/B1C services presents superior performance in both static and kinematic experiments, especially under complex conditions. In the future, a more resilient InRPPP system will be developed based on other types of SSR messages for better performance.

#### Acknowledgements

We would like to thank IGS MGEX for providing multi-GNSS data and products. This work is coordinated within the IAG JWG "5.4 Realtime and post-processed kinematic GNSS positioning: status and perspectives for seafloor and sea-surface positioning".

#### Author contributions

Z.Z. proposed the idea, developed the software, and wrote this paper. H.W. developed the software, worked out the technical details, and wrote this paper. Y.Y. proposed the idea, supervised the study, and modified the manuscript. All authors read and approved the final manuscript.

#### Funding

This study is funded by State Key Laboratory of Geo-Information Engineering and Key Laboratory of Surveying and Mapping Science and Geospatial Information Technology of MNR, CASM (2024-01-07), State Key Laboratory of Spatial Datum, the National Natural Science Foundation of China (42374014, 42004014), and the Fundamental Research Funds for the Central University, and Postgraduate Research & Practice Innovation Program of Jiangsu Province (SJCX24\_0203).

#### Availability of data and materials

The datasets used and analyzed during the current study are available from the corresponding author on reasonable request.

## Declarations

### Competing interests

Yuanxi Yang is an editorial board member for *Satellite Navigation* and was not involved in the editorial review or decision to publish this article. All authors declare that they have no competing interests.

Received: 13 November 2024 Revised: 9 June 2025 Accepted: 9 June 2025

Published online: 07 July 2025

## References

- Bahrami, M., Ffoulkes-Jones, G., Zhang, Q., & Inst, N. (2016). Analysis of SBAS orbit and clock corrections for GPS and their applicability to today's mass market multi-GNSS personal navigation. In: Proceedings of the ION GNSS 2016, Institute of Navigation, Portland Oregon, USA, pp 2766–2776 Sept 2016.
- Chen, J., Zhang, Y., Yu, C., Wang, A., Song, Z., & Zhou, J. (2022). Models and Performance of SBAS and PPP of BDS. *Satellite Navigation* 3, 4.
- China Satellite Navigation Office (CSNO) (2022). Interface specification for signal in space of BeiDou satellite-based augmentation system-Dual-frequency augmentation service signal BDSBAS-B2a.
- Elsobeiey, M., & Al-Harbi, S. (2016). Performance of real-time precise point positioning using IGS real-time service. *GPS Solutions* 20(3), 565–571.
- EUROCAE (2019). Minimum operational performance standard for Galileo/ Global Positioning System/ Satellite-based augmentation system airborne equipment. EUROCAE ED-259.
- Ge, M., Gendt, G., Rothacher, M., Shi, C., & Liu, J. (2008). Resolution of GPS carrier-phase ambiguities in precise point positioning (PPP) with daily observations. *Journal of Geodesy*, 82, 389–399.
- Ge, Y., Wang, Q., Wang, Y., Lyu, D., Cao, X., Shen, F., & Meng, X. (2023). A new receiver clock model to enhance BDS-3 real-time PPP time transfer with the PPP-B2b service. *Satellite Navigation* 4, 8.
- Geng, J., & Bock, Y. (2013). Triple-frequency GPS precise point positioning with rapid ambiguity resolution. *Journal of Geodesy*, 87, 449–460.
- Geng, T., Li, Z., Xie, X., Liu, W., Li, Y., & Zhao, Q. (2022). Real-time ocean precise point positioning with BDS-3 service signal PPP-B2b. *Measurement*, 203, 111911.
- Heßelbarth, A., & Lambert, W. (2013). SBAS orbit and satellite clock corrections for precise point positioning. *GPS Solut*, 17(4), 465–473.
- Hu, Z., Liu, Z., Wang, G., Zhang, Q., Zhou, R., Chen, L., & Zhao, Q. (2023). Initial Performance Assessment of the Single-Frequency (SF) Service with the BeiDou Satellite-Based Augmentation System (BDSBAS). *GPS Solutions* 27: 35.
- Jin, S., & Su, K. (2020). PPP models and performances from single- to quad-frequency BDS observations. *Satellite Navigation* 1, 16.
- Kan, H., Hu, Z., Chen, G., Liu, X., Liu, C., & Zhao, Q. (2024). Performance comparison of orbit and clock augmentation corrections from PPP-B2b. *HAS and CLAS. Advances in Space Research* 74(2), 668–681.
- Kim, E., Song, J., Shin, Y., Kim, S., Son, P. W., Park, S., & Park, S. (2022). Fault-free protection level equation for CLAS PPP-RTK and experimental evaluations. *Sensors*, 22(9), 3570.
- Lan, R., Yang, C., Zheng, Y., Xu, Q., Lv, J., & Gao, Z. (2022). Evaluation of BDS-3 B1C/B2b single/dual-frequency PPP Using PPP-B2b and RTS SSR products in both static and dynamic applications. *Remote Sensing* 14(22), 5835.
- Li, J., Yang, Y., He, H., & Guo, H. (2020). Benefits of BDS-3 B1C/B1I/B2a triple-frequency signals on precise positioning and ambiguity resolution. *GPS Solutions* 24, 100.
- Li, L., Jia, C., Zhao, L., Cheng, J., Liu, J., & Ding, J. (2016). Real-time single frequency precise point positioning using SBAS corrections. *Sensors*, 16(8), 1261.
- Li, X., Ge, M., Dai, X., Ren, X., Fritsche, M., Wickert, J., & Schuh, H. (2015). Accuracy and reliability of multi-GNSS real-time precise positioning: GPS, GLONASS, BeiDou, and Galileo. *Journal of Geodesy*, 89, 607–635.
- Li, B., Zang, N., Ge, H., & Shen, Y. (2019). Single-frequency PPP models: analytical and numerical comparison. *Journal of Geodesy*, 93, 2499–2514.

- Liu, J., Tang, C., Zhou, S., Hu, X., Yang, Y., Yang, J., & Liu, Y. (2022a). The bias in PPP-B2b real-time clock offset and the strategy to reduce it. *Remote Sensing* 14(18), 4569.
- Liu, Y., Yang, C., & Zhang, M. (2022b). Comprehensive analyses of PPP-B2b performance in China and surrounding areas. *Remote Sens.* 14(3), 643.
- Malys, S., & Jensen, P. (1990). Geodetic point positioning with GPS carrier beat phase data from the CASA UNO experiment. *Geophysical Research Letters*, 17(5), 651–654.
- Naciri, N., Yi, D., Bisnath, S., De Blas, F. J., & Capua, R. (2023). Assessment of Galileo High Accuracy Service (HAS) test signals and preliminary positioning performance. *GPS Solutions* 27, 73.
- Nie, Z., Liu, F., & Gao, Y. (2020). Real-time precise point positioning with a low-cost dual-frequency GNSS device. *GPS Solutions* 24, 9.
- Nie, Z., Xu, X., Wang, Z., & Du, J. (2021). Initial assessment of BDS PPP-B2b service: precision of orbit and clock corrections, and ppp performance. *Remote Sensing* 13(11), 2050.
- Nie, Z., Zhou, P., Liu, F., Wang, Z., & Gao, Y. (2019). Evaluation of Orbit, clock and ionospheric corrections from five currently available SBAS L1 services: methodology and analysis. *Remote Sensing* 11(4), 411.
- China Satellite Navigation Office (CSNO) (2020a). BeiDou navigation satellite system signal in space interface control document precise point positioning service signal PPP-B2b (Version 1.0).
- China Satellite Navigation Office (CSNO) (2020b). BeiDou navigation satellite system signal in space interface control document Satellite-Based Augmentation System service signal BDSBAS-B1C (Version 1.0).
- Ouyang, C., Shi, J., Peng, W., Dong, X., Guo, J., & Yao, Y. (2023). Exploring characteristics of BDS-3 PPP-B2b augmentation messages by a three-step analysis procedure. *GPS Solutions*, 27, 119.
- RTCA (2016). Minimum operational performance standards for global positioning system/satellite-based augmentation system airborne equipment. RTCA DO229E.
- Sun, S., Wang, M., Liu, C., Meng, X., & Ji, R. (2023). Long-term performance analysis of BDS-3 precise point positioning (PPP-B2b) service. *GPS Solutions* 27, 69.
- Tang, C., Hu, X., Chen, J., Liu, L., Zhou, S., Guo, R., Li, X., He, F., Liu, J., & Yang, J. (2022). Orbit determination, clock estimation and performance evaluation of BDS-3 PPP-B2b service. *Journal of Geodesy*, 96(9), 60.
- Tao, J., Liu, J., Hu, Z., Zhao, Q., Chen, G., & Ju, B. (2021). Initial Assessment of the BDS-3 PPP-B2b RTS compared with the CNES RTS. *GPS Solut.*, 25, 131.
- Teunissen, P. (2018). Distributional theory for the DIA method. *Journal of Geodesy*, 92, 59–80.
- Wang, H., Zhang, Z., Dong, Y., Zhan, W., & Li, Y. (2024). Real-time multipath mitigation based on spatiotemporal correlations in BDS precise point positioning. *GPS Solutions* 28, 37.
- Wu, M., Wang, L., Xie, W., Yue, F., & Cui, B. (2024). Performance evaluation and application field analysis of precise point positioning based on different real-time augmentation information. *Remote Sensing* 16(8), 1349.
- Xu, P., & Liu, J. (2014). Variance components in errors-in-variables models: Estimability, stability and bias analysis. *Journal of Geodesy*, 88, 719–734.
- Xu, P., Shen, Y., Fukuda, Y., & Liu, Y. (2006). Variance component estimation in linear inverse ill-posed models. *Journal of Geodesy*, 80, 69–81.
- Xu, X., Nie, Z., Wang, Z., Zhang, Y., & Dong, L. (2023). An improved BDS-3 PPP-B2b positioning approach by estimating signal in space range errors. *GPS Solutions* 27, 110.
- Xu, Y., Yang, Y., & Li, J. (2021). Performance evaluation of BDS-3 PPP-B2b precise point positioning service. *GPS Solutions* 25, 142.
- Yang, H., He, X., Ferreira, V., Ji, S., Xu, Y., & Song, S. (2023). Assessment of precipitable water vapor retrieved from precise point positioning with PPP-B2b service. *Earth Science Informatics*, 16(1), 315–328.
- Yang, H., Ji, S., Weng, D., Wang, Z., He, K., & Chen, W. (2021a). Assessment of the feasibility of PPP-B2b service for real-time coseismic displacement retrieval. *Remote Sensing* 13(24), 5011.
- Yang, H., Ren, X., Liu, M., & Zhang, X. (2024). Dual-frequency to five-frequency real-time precise point positioning using new BDS-3 PPP-B2b service. *Earth, Planets and Space*, 76(1), 82.
- Yang, Y. (2019). Resilient PNT concept frame. *Journal of Geodesy and Geoinformation Science*, 2(3), 1–7.
- Yang, Y., Ding, Q., Gao, W., Li, J., Xu, Y., & Sun, B. (2022). Principle and performance of BDSBAS and PPP-B2b of BDS-3. *Satellite Navigation* 3, 5.
- Yang, Y., Gao, W., Guo, S., Mao, Y., & Yang, Y. (2019). Introduction to BeiDou-3 navigation satellite system. *Navigation*, 66(1), 7–18.
- Yang, Y., Liu, L., Li, J., Yang, Y., Zhang, T., Mao, Y., Sun, B., & Ren, X. (2021b). Featured services and performance of BDS-3. *Science Bulletin*, 66(20), 2135–2143.
- Yuan, H., Zhang, Z., He, X., & Wang, H. (2025). Single-station-augmented PPP-B2b considering the satellite-specific clock bias via short-message communication. *Journal of Geodesy*, 99(5), 42.
- Zang, J., Fan, S., Xu, C., Li, Z., Fang, R., & Lou, Y. (2024). Performance assessment of the BDS-3 PPP-B2b service for real-time earthquake source description, a case study for the 2021 Mw 7.4 maduo earthquake. *GPS Solutions* 28, 26.
- Zang, N., Li, B., Nie, L., & Shen, Y. (2020). Inter-system and inter-frequency code biases: simultaneous estimation, daily stability and applications in multi-GNSS single-frequency precise point positioning. *GPS Solutions* 24, 18.
- Zeng, P., Zhang, Z., Wen, Y., He, X., He, L., Li, M., & Chen, W. (2023). Properties of multi-GNSS uncalibrated phase delays with considering satellite systems, receiver types, and network scales. *Satellite Navigation* 4, 19.
- Zhang, B., Zhao, C., Odolinski, R., & Liu, T. (2021). Functional model modification of precise point positioning considering the time-varying code biases of a receiver. *Satell Navig.*, 2, 11.
- Zhang, W., Lou, Y., Song, W., Sun, W., Zou, X., & Gong, X. (2022). Initial assessment of BDS-3 precise point positioning service on GEO B2b signal. *Advances in Space Research*, 69(1), 690–700.
- Zhang, X., Guo, F., & Zhou, P. (2014). Improved precise point positioning in the presence of ionospheric scintillation. *GPS Solutions* 18, 51–60.
- Zhang, Z., Li, X., Yuan, H., & Luo, Y. (2024). An enhanced outlier processing approach based on the resilient mathematical model compensation in GNSS precise positioning and navigation. *Measurement Science & Technology*, 35, 015007.
- Zhang, Z., Li, Y., He, X., & Hsu, L. (2023). Resilient GNSS real-time kinematic precise positioning with inequality and equality constraints. *GPS Solutions* 27, 116.
- Zhang, Z., & Wang, H. (2025). Integrated BeiDou satellite-based augmentation system framework combining B2a and B1C services. *GPS Solutions* 29, 74.
- Zhao, Y., Zhao, L., Li, L., & Yang, F. (2016). A novel SBAS-assisted single-frequency precise point positioning method. *China satellite navigation conference (CSNC) 2016 proceedings* (Vol. III, pp. 373–386). Springer.
- Zhou, H., Wang, L., Fu, W., Han, Y., Li, T., Li, W., & Chen, R. (2022). Real-time single-frequency precise point positioning using BDS-3 PPP-B2b corrections. *Measurement*, 205, 112178.
- Zumberge, J., Heflin, M., Jefferson, D., Watkins, M., & Webb, F. (1997). Precise point positioning for the efficient and robust analysis of GPS data from large networks. *Journal of Geophysical Research-Solid Earth*, 102(B3), 5005–5017.

## Publisher's Note

Springer Nature remains neutral with regard to jurisdictional claims in published maps and institutional affiliations.